On Filtration for High-Energy Phase-Contrast X-ray Imaging

Christian Riess[a], Ashraf Mohamed[b], Waldo Hinshaw[a] and Rebecca Fahrig[a]

[a]Radiological Sciences Laboratory, Stanford University, 1201 Welch Road, Palo Alto, CA, USA
[b]Siemens Medical USA

ABSTRACT

Phase-sensitive X-ray imaging promises unprecedented soft-tissue contrast and resolution. However, several practical challenges have to be overcome when using the setup in a clinical environment. The system design that is currently closest to clinical use is the grating-based Talbot-Lau interferometer (GBI).[1–3]

The requirements for patient imaging are low patient dose, fast imaging time, and high image quality. For GBI, these requirements can be met most successfully with a narrow energy width, high-flux spectrum. Additionally, to penetrate a human-sized object, the design energy of the system has to be well above 40 keV. To our knowledge, little research has been done so far to investigate optimal GBI filtration at such high X-ray energies.

In this paper, we study different filtration strategies and their impact on high-energy GBI. Specifically, we compare copper filtration at low peak voltage with equal-absorption, equal-imaging time K-edge filtration of spectra with higher peak voltage under clinically realistic boundary conditions. We specifically focus on a design energy of 59 keV and investigate combinations of tube current, peak voltage, and filtration that lead to equal patient absorption. Theoretical considerations suggest that the K edge of tantalum might provide a transmission pocket at around 59 keV, yielding a well-shaped spectrum. Although one can observe a slight visibility benefit when using tungsten or tantalum filtration, experimental results indicate that visibility benefits most from a low X-ray tube peak voltage.

Keywords: Grating-based phase contrast X-ray, spectrum filtration, X-ray filtration, k-edge filtration

1. INTRODUCTION

Phase-sensitive X-ray imaging is attracting increasing attention in the medical community. In theory, this new modality can yield greatly improved soft-tissue contrast. However, when using a phase-sensitive setup in a clinical environment, several practical challenges must be overcome, particularly considering the setup's complexity, constraints on imaging time and image quality. The system design that is currently closest to clinical use is the grating-based Talbot-Lau interferometer.[1–4]

Considerable effort has been invested in understanding the impact of various interferometer parameters on image quality.[2,5,6] The choice of the X-ray spectrum also has a big effect on image quality. However, to our knowledge, only a little research has been done on the filtration of the GBI spectrum.[7] The reason that this topic has been overlooked may be because up until now, most grating-based phase-contrast systems were operated at X-ray energies in the range of 20 keV to 40 keV. Here, beam filtration is straightforward. However, for tasks in medical diagnosis, it is likely that phase-contrast X-ray energies must be increased. In this case, proper beam filtration is expected to be more challenging. In this paper, we report first experiments and considerations towards effective X-ray beam filtration for a higher energy setup. We compare copper filtration with different K-edge filters. We use the commonly used fringe visibility as a figure of merit. For the experiments, the tube flux is controlled, such that a water phantom is always absorbing approximately the same amount of energy. Under these conditions, thin sheets of tantalum or tungsten filters may indeed improve the visibility at 59 keV. However, most important for obtaining good visibility is to keep the tube's peak voltage low.

Further author information: (Send correspondence to Rebecca Fahrig)
Rebecca Fahrig: E-mail: fahrig@stanford.edu, Telephone: 1 (650) 726-6923

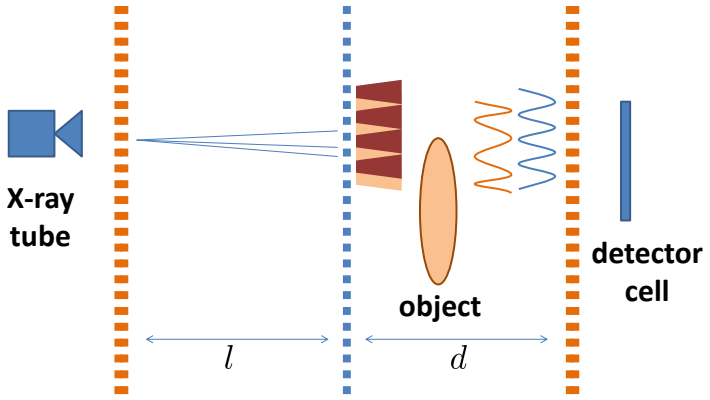

Figure 1: Sketch of a grating-based X-ray phase contrast system. Viewed from the top. Beam direction is from left to right. See text for details.

2. METHODS

A sketch of a grating-based phase contrast system is shown in Fig. 1. The system consists of an off-the-shelf medical X-ray tube (e. g., with a rotating tungsten anode) and a standard medical X-ray detector (e. g., a CsI flat panel detector). Between source and detector, three gratings $G0$, $G1$, $G2$ are mounted with inter-grating distances l and d (for details, see[4]). The leftmost grating $G0$ ("source grating") is usually made of gold for ease of manufacturing and its high X-ray absorption. It splits the X-ray beam into an array of smaller sources. Each of these sources is sufficiently coherent for use in the interferometer. The second grating $G1$ ("phase grating") is mostly transparent to the X-rays. On the grating bars, the phase of incident X-rays is shifted. A common design choice for the phase shift factor is π.[4] The X-rays interfere and form a so-called Talbot self image of $G1$ at specific Talbot distances d downstream of $G1$ (indicated as a blue sinusoid in Fig. 1). If a specimen (or patient) is placed in the beam path, different materials shift the phase of the wave front differently, which leads to a distortion of the wave front (indicated as an orange sinusoid). The distortion can be measured using a procedure called phase stepping. Here, the wavefront is scanned by capturing a series of images while moving grating $G2$ ("analyzer grating") perpendicularly to the grating bars.

A medical tungsten anode X-ray tube produces a broad spectrum of polychromatic X-ray radiation. The contribution to the image contrast greatly differs for various wavelengths of the spectrum. The contrast is maximum at the design energy of the system, which depends on the distances l and d. The contrast per wavelength in the neighborhood of the design energy can be approximated as a sinusoid.[4]

The overall goal of GBI filtration is to concentrate the beam spectrum at or around the design energy of the system. For a clinical X-ray tube with a tungsten anode, a straightforward strategy for filtration is to set the peak energy of the tube slightly higher than the design energy of the system, and use a low-Z filter (like aluminum or copper) to prefilter photons at energies significantly below the design energy. However, it is not clear whether this approach scales well to higher X-rays energies. For patient imaging, one can reasonably assume that the GBI design energy should be considerably higher than 40 keV.[8] Prior studies have explored imaging at X-ray energies up to 100 keV.[9,10] However, shaping the spectrum of a clinical tube with a tungsten anode at high design energies may be increasingly difficult with the straightforward approach. Fig. 2 shows a number of spectra, generated with the `spektr` software package by Siewerdsen *et al.*,[11] and copper and tantalum applied as examples of a low-Z and a high-Z filter (also called K-edge filter). The design energy of 59 keV that we focus on in this paper is marked with a vertical line. Since the absorption profiles of low-Z filters fall off slowly at high energies, the relative photon counts of the high-energy portion of the spectrum remain largely unaffected by the filter. Conversely, a filtration material consisting of a high-Z material, e. g., tantalum, tungsten (or, at very high

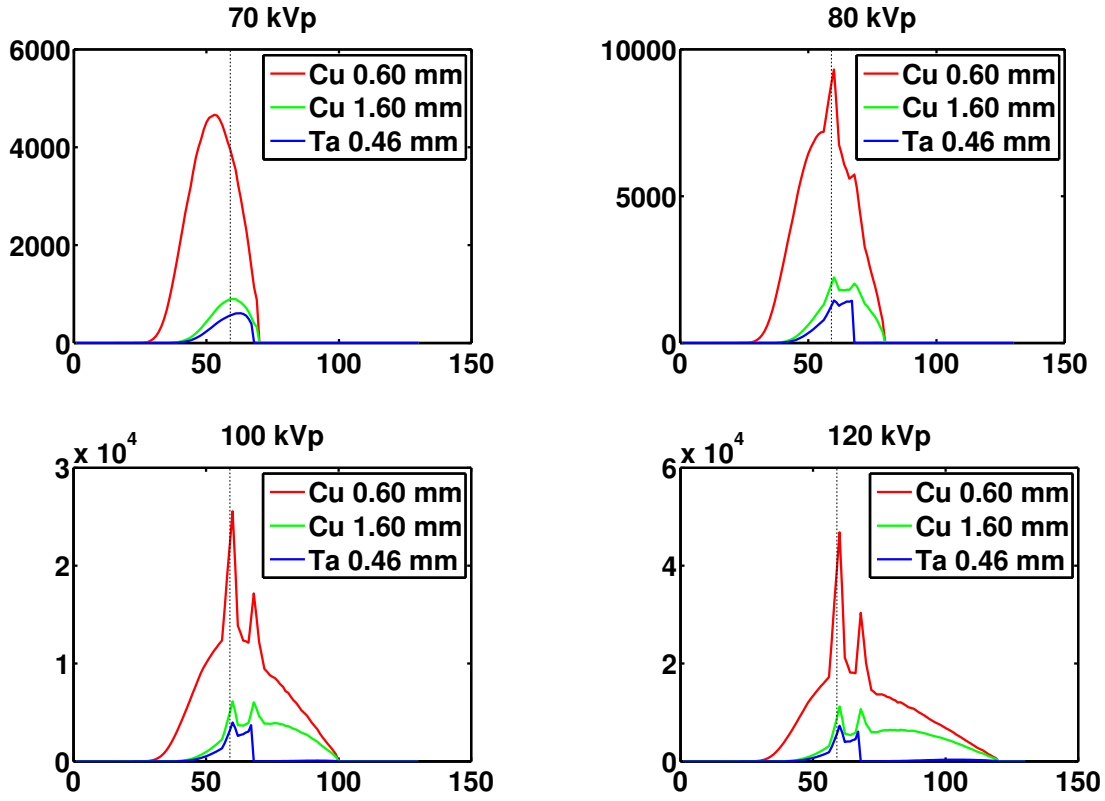

Figure 2: Analytical filtration at 70 keV, 80 keV, 100 keV, and 120 keV peak energy. The investigated design energy of 59 keV is marked by the vertical line.

design energies, lead) sharply cuts off the part of the spectrum above their K edge. Just below their K edge, a "transmission pocket" exists that may be useful for shaping a narrow spectrum close to that energy. On the downside, the overall absorption of K-edge filters is very high. To obtain sufficient photon flux for imaging, it is necessary to apply a higher current and/or higher peak voltage to the X-ray tube. For instance, the K edge of tantalum is at 67 keV. If the design energy of a GBI system is 59 keV, there is a 8 keV transmission pocket between design energy and the K edge.

The purpose of this study is to investigate whether spectrum filtration close to a K-edge leads to improved fringe visibility. One challenge in such an investigation is to ensure that the comparison of different filtrations is fair. We consider a comparison of two filters fair if the specimen (or patient, respectively) is exposed to the same radiation dose. As a consequence, the X-ray exposure has to be reduced for weakly absorbing filters, or increased for strongly absorbing filters. Accurately estimating the beam adjustment factor that achieves equal dose requires a Monte Carlo simulation. However, we limit our study to an approximation of patient dose by considering cases of *equal absorption* in a defined absorption target.

We now define the constraint of equal X-ray absorption more precisely. Denote each investigated spectrum filtration with an index number i. For the i-th filter $f_i(e, l_i)$ of thickness (length) l_i, the transmission coefficient under a monochromatic X-ray beam with energy e is

$$f_i(e, l_i) = \exp(-\mu_i(e) \cdot l_i) \ , \tag{1}$$

where $\mu_i(e)$ denotes the attenuation coefficient of filter i at energy e. Analogously, let $a(e)$ denote the transmission coefficient of 5.8 cm water,

$$w(e) = 1 - f_w(e, 5.8\,\text{cm}) = 1 - \exp(-\mu_w(e) \cdot 5.8\,\text{cm}) \ , \tag{2}$$

where $\mu_w(e)$ denotes the attenuation coefficient of water at energy e. The absorption $a(i)$ of a spectrum S_i in 5.8 cm water behind a filter f_i is

$$a(i) = c_i t_i \cdot \int_{e \in S_i} n(e) \cdot f_i(e, l_i) w(e) de \ , \tag{3}$$

where c_i denotes the tube current in mA, t_i denotes the exposure time in seconds, and $n(e)$ denotes the normalized number of photons at energy e. For two filters f_i, f_j operating on two X-ray spectra S_i, S_j, the constraint of equal X-ray absorption can be enforced by manipulating current and exposure time in one of the filters. Specifically, we introduce an energy-independent absorption correction factor h, such that

$$a(i) = h \cdot a(j) \ , \tag{4}$$

which can be satisfied by adjusting tube current and exposure time

$$c_i \cdot t_i = h \cdot c_j \cdot t_j \ . \tag{5}$$

If the X-ray exposure times t_i, t_j are fixed and constant, i. e., $t = t_i = t_j$, the correction factor h only influences the tube current.

In our specific case, we assume that the X-ray beam is created by a tungsten rotating-anode X-ray tube. The peak voltage of the X-ray tube may vary between 70 kVp and 120 kVp in steps of 10 kVp. The time for a single X-ray exposure is fixed at 20 ms or 40 ms, respectively (see further information below). The tube current is varied between 20 mA and 80 mA. The X-ray beam is filtered with 0.6 mm and 1.6 mm of copper, 0.1 mm and 0.2 mm of tungsten, and 0.15 mm, 0.2 mm, 0.3 mm, and 0.4 mm of tantalum. The target for equal X-ray absorption was about 5.8 cm of water in a negligibly thin PMMA cup.

Table 1 shows calculations of the current if the exposure time is fixed. In practice, our X-ray tube allows only a maximum of 80 mA in fluoroscopy mode. To image scenarios where Tab. 1 requires currents above 80 mA, we use the exposure time of 40 ms instead of 20 ms, which allows us to halve the current.

We use these configurations to investigate the expected visibilities. The visibility of a GBI system is one of the integral quality parameters[5,6] and is defined for the stepping curve of a single pixel as

$$V = \frac{I_{\max} - I_{\min}}{I_{\max} + I_{\min}} \ , \tag{6}$$

where $I_{\min}$ and $I_{\max}$ are the minimum and maximum intensities of the stepping curve, respectively. The average visibility of an image is the mean value of the per-pixel visibilities.

Our experimental setup has a design energy of 59 keV, and consists of a π-shifting nickel phase grating G1 with a period of 4.8 µm. The two gold absorption gratings G0 and G2 have a height of about 190 µm and a period of 4.8 µm. All duty cycles are 0.5. The setup geometry is symmetric. We report experiments with grating distances at the first and third fractional Talbot orders, i. e., at distances of 27.41 cm and 82.23 cm, respectively, between each pair of gratings. The setup includes a Varian G-1593BI rotating anode X-ray tube at fluoro settings and a Varian Paxscan flat panel detector with a binning of 2×2 pixels.

The experimental protocol starts with a (manual) geometric grating calibration using an X-ray beam filtration of 0.6 mm copper at 70 kVp with subsequent imaging of the 5.8 cm water sample and another reference scene. The other investigated filter/kVp configurations are then set up without changing the geometric calibration. The order of the measurements is to mount the filters in the order as given in Tab. 1. For each mounted filtration, the calculated tube voltages were applied in increasing order. After a change of filtration or peak voltage, the detector gain and offset are recalibrated. In traditional X-ray radiographs, it is important to remove any objects from the beam path during gain calibration. However, the phase stepping still provides meaningful results if the gratings are still within the field of view during gain calibration. This makes it possible to maintain the same geometric calibration across experiments with different filtrations and kVp.

Filtration	70 kVp	80 kVp	90 kVp	100 kVp	110 kVp	120 kVp
0.6 mm Cu	80 mA					
1.6 mm Cu			78 mA	41 mA		
0.1 mm W	59 mA					
0.2 mm W		82 mA	51 mA			
0.15 mm Ta	82 mA	42 mA				
0.2 mm Ta	130 mA	65 mA	41 mA			
0.3 mm Ta		138 mA	86 mA	59 mA	42 mA	
0.4 mm Ta				116 mA	84 mA	61 mA

Table 1: Adjustment factors for obtaining for each filtration at each peak energy the same absorption in a sample of 5.8 cm water. The tabulated numbers display how the X-ray tube's Ampere settings have to be adjusted if the exposure time is fixed.

3. RESULTS AND DISCUSSION

Table 2 shows experimentally obtained visibilities at first fractional Talbot order. The same experiments have been repeated at third fractional Talbot order, which is reported in Tab. 3. For a detection task, the main advantage of third fractional Talbot order lies in the potentially higher setup sensitivity. However, in our case, only the fringe contrast is measured. There are two main differences between the first and third fractional Talbot orders. First, due to the much larger source-detector distance at third fractional Talbot order, it is more difficult to obtain sufficient photon statistics at the detector, i. e., the obtained X-ray image is much darker. Second, smaller fractional Talbot order allows a broader part of the X-ray spectrum to contribute to the fringe visibility.[4]

The data in Tab. 2 is the result of a single, uninterrupted experimental session. In Tab. 3, several datapoints have minor errors. For the 1.6 mm copper filtration, the mA settings on the tube were 10 kV too low, leading to a more compact spectrum with a relatively lower number of photons than for the other cases. Additionally, the geometric calibration had to be renewed for the measurements of 0.3 mm tantalum at 80 kVp and 0.4 mm tantalum at 110 kVp.

While there is some variability in the measured values, there are also trends that are apparent from the measured visibilities in Tab. 2 as well as in Tab. 3.

The most important observation is that for a given filtration, a lower tube voltage almost always leads to better visibility. Across the tables, the measured visibility only increases with the tube voltage in four cases. At first fractional Talbot order, visibility increases for 0.2 mm tantalum between 80 kVp and 90 kVp, and for 0.3 mm tantalum between 100 kVp and 110 kVp. At third fractional Talbot order, visibility also increases for 0.3 mm tantalum between 100 kVp and 110 kVp, and additionally for 0.4 mm tantalum between 110 kVp and 120 kVp. However, in the vast majority of cases, higher visibilities are obtained with lower tube voltages.

A second observation is that there is some indication of a slight benefit of K-edge filtration when combined with a low-energy spectrum. More specifically, at first fractional Talbot order, all cases of K-edge filters operated at 70 kVp obtained comparable or even higher visibilities than the copper filtration at 70 kVp. At third fractional Talbot order, only 0.1 mm tungsten at 70 kVp achieve a visibility that is comparable to copper.

Considering, e. g., the shape of the filtered X-ray spectra in Fig. 2, the impact of the K-edge filter is surprisingly small. Instead, experimental results indicate that it is always beneficial to start with a low X-ray peak voltage, and consider its filtration as a secondary refinement.

One possible explanation for this finding is that the plots in Fig. 2 do not consider tube current or exposure time. For the experimental data, we carefully enforced the equal-absorption constraint, and were limited in the X-ray voltages by the maximum tube current. Considering the tube currents required for the equal-absorption constraint in Tab. 1, only thin K-edge filters are practical at low tube voltages if the imaging time is limited. Thus, in a realistic scenario, a K-edge filter can shape an X-ray spectrum only to a certain extent. If these conditions are met, it turns out that K-edge filtration is advantageous if the tube current can be tuned up to compensate for the higher absorption of the filtration at low peak voltages.

Filtration	70 kVp	80 kVp	90 kVp	100 kVp	110 kVp	120 kVp
0.6 mm Cu	5.78%					
1.6 mm Cu			4.18%	2.46%		
0.1 mm W	6.29%					
0.2 mm W		4.53%	3.91%			
0.15 mm Ta	5.79%	5.04%				
0.2 mm Ta	6.53%	4.19%	4.93%			
0.3 mm Ta		5.69%	5.16%	4.39%	3.84%	
0.4 mm Ta				4.46%	3.74%	3.64%

Table 2: Experimentally obtained visibilities with equal X-ray absorption in 5.8 cm water at first fractional Talbot order.

Filtration	70 kVp	80 kVp	90 kVp	100 kVp	110 kVp	120 kVp
0.6 mm Cu	5.45%					
1.6 mm Cu		(3.46%*)	(3.08%*)			
0.1 mm W	5.49%					
0.2 mm W		4.17%	3.58%			
0.15 mm Ta	5.05%	4.59%				
0.2 mm Ta	5.01%	4.69%	3.76%			
0.3 mm Ta		5.20%†)	4.66%	4.18%	4.23%	
0.4 mm Ta				4.34%	4.19%†)	4.28%

Table 3: Experimentally obtained visibilities with equal X-ray absorption in 5.8 cm water at third fractional Talbot order. *) tube peak voltage was set 10 kV too low. †) setup was geometrically recalibrated for this measurement.

One weakness of our experimental protocol is the sequential evaluation of the filtration/kVp combinations, because the gratings are only calibrated geometrically after the first configuration (0.6 mm copper). This may give rise to two types of error. First, later configurations may be penalized by a drift in the calibration due to heat, vibrations, or slightly unstable mounts. Second, the calibration may overfit the particular filtration/kVp configuration for which it is conducted. We addressed both points by repeating selected measurements in different orders to support the two central observations reported in this paper.

4. CONCLUSIONS

We present a comparison of X-ray spectrum filtration with copper versus tantalum for high-energy grating-based phase-contrast X-ray (GBI). Since tantalum and tungsten exhibit K edges between 60 keV and 70 keV, they may be suitable candidates for beam filtration of a GBI system with design energies at or around 59 keV. We report a series of experiments in which copper, tantalum, and tungsten were compared. To ensure the fairness of the comparison, the tube is set up such that the absorption of all filtered beams in 5.8 cm water is approximately the same. We limit ourselves to configurations of filtrations, tube currents and voltages that are feasible to compare on a typical medical X-ray tube and detector. It turns out that for each filtration, lower peak voltages consistently produces better visibilities. At the same time, lower peak voltages require an increase in the tube current to obtain sufficiently high photon counts. This leads to an interesting conclusion about K-edge filters: if the X-ray tube produces sufficient current to operate a K-edge filter at low peak voltage, there may be a benefit in K-edge filtration. Otherwise, our results indicate that traditional beam filtration is preferred.

REFERENCES

[1] Momose, A., Koyama, I., Hamaishi, Y., Takai, K., and Suzuki, Y., "Demonstration of x-ray talbot interferometry," *Japanese Journal of Applied Physics* **42**, L866–L868 (July 2003).

[2] Weitkamp, T., Diaz, A., David, C., Pfeiffer, F., Stampanoni, M., Cloetens, P., and Ziegler, E., "X-ray Phase Imaging with a Grating Interferometer," *Optics Express* **12**, 6296–6304 (Aug. 2005).

[3] Pfeiffer, F., Weitkamp, T., Bunk, O., and David, C., "Phase Retrieval and Differential Phase-contrast Imaging with Low-brilliance X-ray Sources," *Nature Physics* **2**, 258–261 (Apr. 2006).

[4] Weitkamp, T., David, C., Kottler, C., Bunk, O., and Pfeiffer, F., "Tomography with Grating Interferometers at Low-Brilliance Sources," in [*Proceedings of the SPIE — Developments in X-Ray Tomography*], **6318**, 63180S–1 (Aug. 2006).

[5] Revol, V., Kottler, C., Kaufmann, R., Straumann, U., and Urban, C., "Noise analysis of grating-based x-ray differential phase contrast imaging," *Review of Scientific Instruments* **81**(7), 073709–1–073709–7 (2010).

[6] Weber, T., Bartl, P., Durst, J., Haas, W., Michel, T., Ritter, A., and Anton, G., "Noise in x-ray grating-based phase-contrast imaging," *Medical Physics* **38**, 4133–4140 (July 2011).

[7] Weber, T., Bayer, F., Gödel, K., Haas, W., Pelzer, G., Rieger, J., Ritter, A., Wucherer, L., Durst, J., Michel, T., and Anton, G., "Spectrum optimization of a talbot-lau interferometer towards clinical application," in [*Proceedings of the SPIE 8313, Medical Imaging 2012: Physics of Medical Imaging*], **83135F** (Feb. 2012).

[8] Sarapata, A., Stayman, J. W., Finkenthal, M., Siewerdsen, J. H., Pfeiffer, F., and Stutman, D., "High energy x-ray phase contrast ct using glancing-angle grating interferometers," *Medical Physics* **41**, 021904–1–021904–9 (Feb. 2014).

[9] Thüring, T., Abis, M., Wang, Z., David, C., and Stampanoni, M., "X-ray phase-contrast imaging at 100 keV on a conventional source," *Scientific Reports* **4**, 5198 (June 2014).

[10] Willner, M., Bech, M., Herzen, J., Zanette, I., Hahn, D., Kenntner, J., Mohr, J., Rack, A., Weitkamp, T., and Pfeiffer, F., "Quantitative X-Ray Phase-Contrast Computed Tomography at 82 keV," *Optics Express* **21**, 4155–4166 (Feb. 2013).

[11] Siewerdsen, J. H., Waese, A. M., Moseley, D. J., Richard, S., and Jaffray, D. A., "Spektr: A computational tool for x-ray spectral analysis and imaging system optimization," *Medical Physics* **31**, 3057–3067 (Nov. 2004).